Molecular Genetics and Metabolism 145 (2025) 109150

Contents lists available at ScienceDirect

Molecular Genetics and Metabolism

journal homepage: www.elsevier.com/locate/ymgme

Research Paper

Missense mutations in MMACHC protein from *cblC* disease affect its conformational stability and vitamin B12-binding activity: The example of R161Q mutation

Lisa Longo [a,b], Loredana Randazzo [a], Michela Bollati [c], Rita Carrotta [a], Maria Assunta Costa [a], Matteo De Rosa [c], Maria Rosalia Mangione [a], Vincenzo Martorana [a], Giulia Culletta [b], Marco Tutone [b], Eleonora Mari [d], Maria Grazia Ortore [d], Paula M. Garcia-Franco [e,f], Adrian Velazquez-Campoy [e,g,h,i], Rosa Passantino [a,*], Silvia Vilasi [a,*]

[a] *Institute of Biophysics, National Research Council, 90146 Palermo, Italy*
[b] *Department STEBICEF, University of Palermo, 90128 Palermo, Italy*
[c] *Institute of Biophysics, National Research Council, 20133 Milano, Italy*
[d] *Department of Life and Environmental Sciences, Polytechnic University of Marche, Ancona, Italy*
[e] *Institute of Biocomputation and Physics of Complex Systems (BIFI), Universidad de Zaragoza, 50018 Zaragoza, Spain*
[f] *Certest Biotec S.L., 50840 San Mateo de Gallego, Zaragoza, Spain*
[g] *Institute for Health Research Aragon (IIS Aragon), 50009 Zaragoza, Spain*
[h] *Networking Biomedical Research Centre in Liver and Digestive Diseases (CIBERehd), 28029 Madrid, Spain*
[i] *Department of Biochemistry and Molecular and Cell Biology, University of Zaragoza, 50009 Zaragoza, Spain*

ARTICLE INFO

Keywords:
MMACHC protein
cblC disease
Thermodynamics
Oligomeric equilibrium
Cobalamin binding
Osmolytes

ABSTRACT

MMACHC protein plays a crucial role in the metabolism of vitamin B12 (cobalamin, Cbl) by catalyzing its conversion into the active forms adenosylcobalamin (AdoCbl) and methylcobalamin (MeCbl), which serve as essential cofactors in key cellular reactions. Mutations in the gene encoding MMACHC lead to the rare metabolic disorder known as methylmalonic aciduria and homocystinuria, cblC type. This condition predominantly affects children and is characterized by cardiovascular dysfunction, intellectual disability, and a severe form of maculopathy. The most common missense mutation, R161Q, impairs enzymatic activity despite not being directly involved in cobalamin binding. Here, using a comprehensive set of biophysical techniques, we demonstrate that this pathogenic variant compromises MMACHC structural stability, alters the thermal unfolding cooperativity and pathway, as well as the populations of conformational intermediates. Moreover, we show that the R161Q mutation decreases AdoCbl binding affinity and impairs the protein's ability to form homodimers, which are supposed to have a functional role. A partial recovery in protein activity upon treatment with betaine, an osmolyte known for its stabilizing effect on proteins, was observed. This suggests a direct correlation between the energetics of MMACHC thermal unfolding and its functional activity. These findings contribute to a deeper understanding of the molecular mechanisms underlying MMACHC function and open avenues for potential therapeutic interventions.

1. Introduction

Methylmalonic aciduria and homocystinuria, cblC type, is a rare disorder arising from a malfunction in the metabolism of vitamin B12 (cobalamin, Cbl). Specifically, cblC disorder results from mutations, numbering more than sixty, within the gene which encodes MMACHC protein, responsible for transporting and processing various Cbl derivatives [1–3]. Specifically, a key function of MMACHC is to catalyse the removal of the upper axial ligand from different Cbl forms, AdoCbl, MeCbl, CNCbl (cyanocobalamin), and OHCbl (hydroxocobalamin), with the help of specific cofactors, such as reduced glutathione (GSH) for dealkylation and flavin mononucleotide/flavin adenine dinucleotide (FMN/FAD) and NADPH for reductive decyanation. These enzymatic activities are essential for the conversion of Cbl into its active forms,

* Corresponding authors at: Via Ugo La Malfa, 153, 90146 Palermo, Italy.
E-mail addresses: rosa.passantino@cnr.it (R. Passantino), silvia.vilasi@cnr.it (S. Vilasi).

https://doi.org/10.1016/j.ymgme.2025.109150
Received 15 April 2025; Received in revised form 19 May 2025; Accepted 21 May 2025
Available online 22 May 2025

AdoCbl and MeCbl, which are cofactors for mitochondrial methylmalonyl-CoA mutase (MUT) and cytosolic methionine synthase (MS), respectively [4,5]. Given that MUT catalyzes the transformation of methylmalonyl-CoA (mmCoA) to succinyl-CoA and MS the conversion of homocysteine (Hcy) into methionine, mmCoA and Hcy abnormally accumulate in the body of cblC patients. The clinical implications of cblC disorder are severe and systemic, encompassing pulmonary issues, hemolytic-uremic syndrome, neuro-cognitive deficits, and degenerative maculopathy [6–9]. Presently, the primary treatment for cblC involves the intramuscular injections of highly concentrated hydroxocobalamin (OHCbl), administration of L-carnitine, folic acid and betaine [10], the latter of which has been shown to be an effective agent for decreasing plasma homocysteine in healthy adults [11]. However, long-term management of affected individuals often proves unsatisfactory, as neurological and ocular impairments tend to progress despite treatment.

The most prevalent allelic variant observed in cblC patients is c.271dupA, a mutation which is hypothesized to trigger nonsense-mediated mRNA decay (NMD) and that would lead to the production of a truncated protein p.Arg91Lysfs*14 with a 14-amino acid frameshift. For this mutation, gene therapy or enzyme replacement approaches appear to be the only viable therapeutic options. Conversely, mutations that still allow the production of MMACHC protein may offer opportunities for alternative affordable strategies, such as pharmacological interventions. Nevertheless, deciphering the precise impact of each pathological mutation on the resultant MMACHC protein structure and function is paramount for designing effective treatments.

From a structural point of view, MMACHC is composed by an alpha/beta N-terminal domain folded to form, at the interface with the 4 helices C-terminal region, a large pocket which perfectly accommodates cobalamin [12,13].

A cluster of three arginine residues, including the one at position 161, is involved in GSH binding and therefore in the dealkylation process. While in the absence of any ligand the apoprotein is monomeric [12], structural studies revealed the existence of MMACHC dimers upon incubation with AdoCbl, suggesting a monomer/dimer equilibrium [13]. In the proposed dimeric model, a protrusion from one subunit extends across and interacts with the deoxyadenosine moiety of AdoCbl in the opposite subunit. MMACHC is a multifunctional enzyme, with different activities regulated by binding to Cbl and other cofactors, and likely by the formation of the domain-swapped dimers. Understanding how a pathological mutation impacts these different aspects is important for identifying effective therapies and, more broadly, for gaining a clearer comprehension of the still uncertain mechanisms underlying the protein's function.

In this study, using the pathological mutant R161Q, resulting from c.482G > A mutation, we show how a biophysical approach can address some key questions concerning the structure/function relationship of pathological proteins resulting from mutations in the MMACHC gene. Specifically, our aim was to assess the chemico-physical properties of the protein and how these properties, when affected by the pathological mutation, correlate with its dysfunction. The R161Q substitution was shown to impair the binding to the cofactor GSH with a significant decrease in dealkylation activity [13,14]. Moreover, the mutation was also shown to have a considerable effect on the global stability of the protein [15]. Indeed the R161Q mutant showed a shift in the unfolding temperature (T_m) compared to the wild-type (WT) protein, interpreted through a two-state unfolding model using differential scanning fluorimetry [15]. Here, using differential scanning calorimetry (DSC) and circular dichroism (CD), we were able to uncover a more complex MMACHC thermal unfolding process, showing the existence, in both proteins, of two distinct thermal transitions and revealing important differences in the unfolding energetic pathways between the wild type and the mutant. These changes were found to correlate with alterations in protein structure, cobalamin-binding ability, and oligomer arrangement, as assessed using complementary biophysical and biochemical techniques, including isothermal titration calorimetry (ITC), native gel electrophoresis, size sxclusion chromatography (SEC), small-angle X-ray scattering (SAXS) and light scattering (LS), and enzymatic assays. The influence of the point mutation on MMACHC global stability suggests that the folding rescue, which was revealed to be a promising therapeutic route [16–20] for mutations affecting protein folding/stability properties, could also have an impact in the cblC therapeutic approach.

Hence, as a proof-of-concept, we also evaluated the ability of different osmolytes to stabilize MMACHC-WT and MMACHC-R161Q protein using isothermal denaturation fluorimetry. Our findings revealed that only betaine exhibited a stabilizing effect on the proteins, partially improving R161Q mutant activity. Taken together, these findings could have implications in the development of therapeutic approaches based on protein stabilization strategies in cblC treatment.

2. Materials & methods

2.1. Plasmids and site-directed mutagenesis

The plasmid pNIC28-Bsa4-MMACHC expressing the human MMACHC-WT as a TEV protease cleavable N-terminal His-tag protein was a gift from Nicola Burgess-Brown (Addgene plasmid # 39096; http://n2t.net/addgene:39096; RRID: Addgene_39,096). Mutant sequence was generated by site-directed mutagenesis of the wild-type vector using QuikChange Lightning Site-Directed Mutagenesis Kit (Agilent Technologies, Inc.) and the primers GCTGGTTTGCCATC-CAA**G**GGGTAGTGCTGCT and AGCAGCACTACCCC**T**TGGATGGCAAAC-CAGC, where the letters in bold represent the mutated nucleotides. The resulting plasmid pNIC28-Bsa4-MMACHC-R161Q leads to the expression of MMACHC-R161Q, a protein where the arginine residue in position 161 is substituted by a glutamine. The nucleotide sequence was confirmed by Sanger sequencing.

2.2. Expression and purification of MMACHC-WT and MMACHC-R161Q

Expression and purification of recombinant MMACHC-WT and MMACHC-R161Q proteins were carried out following the procedure previously described, with minor modifications [21]. Briefly, *Escherichia coli* BL21-Gold (DE3) harboring pNIC28-Bsa4-MMACHC was grown at 37 °C in Terrific Broth (TB) medium supplemented with kanamycin (30 μg/mL). When OD600 of the culture reached 2, expression was induced by addition of 0.1 mM isopropyl 1-thio-β-d-galactopyranoside (IPTG) overnight at 18 °C. Upon harvesting, cells were suspended in pre-chilled lysis buffer 20 mM PB (10 mM Na2HPO4, 10 mM NaH2PO4) pH 7.4, 0.5 M NaCl, supplemented with 25 U/mL Benzonase ® (Merk-Millipore), 5 mM $MgCl_2$, 0.4 mg/mL lysozyme, one tablet of cOmplete™ EDTA-free protease inhibitor mixture (Roche), 5 % (*v*/v) glycerol and 10 mM imidazole. The cells were disrupted on ice by sonication (Bandelin HD 2070) and the supernatant was collected after centrifugation at 20.000 *g*, 4 °C for 30 min, filtered using 0.2 μm filter, and loaded onto a 5 mL HiTrap TALON crude (Cytiva) column equilibrated in the same buffer of the protein sample. The His-tagged protein was eluted, on a FPLC ÄKTA Primeplus GE Healthcare, with a linear gradient from 10 to 300 mM of imidazole in 10 CV at room temperature, using prechilled elution buffers. A buffer exchange was then obtained using a HiPrep Desalting 26/10 column (Cytiva).

Purity of both proteins was verified by SDS-PAGE using NZYtech BlueSafe as stainer. Proteins were stored in 20 mM PB, pH 7.4, 0.3 M NaCl, 5 % (*v*/v) glycerol, at −80 °C.

2.3. Differential scanning calorimetry (DSC)

The thermal stability of apo MMACHC-WT (17 μM) and apo MMACHC-R161Q (17 μM) was assessed by differential scanning calorimetry in a MicroCal VP-Capillary DSC (MicroCal, Malvern-Panalytical). The partial molar heat capacity at constant pressure of

the protein solution was measured as a function of the temperature at a scanning rate of 1 °C/min. Several buffer-buffer scans were performed to ensure proper instrument and sample equilibration. After instrumental buffer baseline subtraction and concentration normalization, a baseline calculated from the progress of the unfolding process was subtracted to obtain the excess molar heat capacity of the protein.

The thermograms obtained for both MMACHC-WT and MMACHC-R161Q were analyzed applying a two-transition unfolding model using Origin7 package implemented in our laboratory.

In the case of n independent transitions, each one characterized by the three unfolding parameters (unfolding temperature T_m, unfolding enthalpy $\Delta H(T_m)$, and unfolding heat capacity ΔC_P), the excess average heat capacity is given by:

$$\langle \Delta C_P \rangle = \sum_{i=1}^{n} \frac{K_i(T)}{(1+K_i(T))^2} \frac{\Delta H_i(T)^2}{RT^2} \tag{1}$$

where the parameters are defined as in the previous equations:

$$\begin{aligned} K_i(T) &= exp\left(-\frac{\Delta G_i(T)}{RT}\right) \\ \Delta H_i(T) &= \Delta H_{mi} + \Delta C_{P,i}\left(T - T_{m,i}\right) \end{aligned} \tag{2}$$

and using $n = 2$ will correspond to the two-transition unfolding model. The partition function for the model with two independent transitions is written as a product of two elemental sub-partition functions:

$$Z(T) = (1+K_1(T))(1+K_2(T)) \tag{3}$$

with each factor representing a certain region or domain folding independently within the protein molecule, and it can be considered as a global partition function:

$$Z(T) = 1 + K_1(T) + K_2(T) + K_1(T)K_2(T) \tag{4}$$

corresponding to a conformational landscape with four conformational states: folded state, first intermediate state, second intermediate state, and unfolded state. From $Z(T)$ the population of each state as a function of temperature can be calculated as follows:

$$\begin{aligned} P_F(T) &= \frac{1}{Z(T)} \\ P_{I1}(T) &= \frac{K_1(T)}{Z(T)} \\ P_{I2}(T) &= \frac{K_2(T)}{Z(T)} \\ P_U(T) &= \frac{K_1(T)K_2(T)}{Z(\mathrm{T})} \end{aligned} \tag{5}$$

2.4. Circular dichroism

CD spectroscopic measurements were made by using a Chirascan v100 spectrometer (Applied Photophysics) equipped with a temperature control unit.

A quartz cell with a path length of 1 mm was used for recording at 20 °C far-UV (190–250 nm) spectra of the MMACHC-WT (10 μM) and MMACHC-R161Q (10 μM) protein in the absence and in the presence of AdoCbl (Sigma Aldrich) in a molar ratio AdoCbl to protein of 2:1. The concentration of the cobalamin was calculated considering the extinction molar coefficient according to [22]. Spectra were acquired with a 5 nm/min scan rate, band width 3 nm, response 32 s and data pitch 0.5 nm.

The analysis of thermal denaturation was monitored by measuring the ellipticity values at 222 nm upon gradually heating from 15 °C to 90 °C for both the MMACHC-WT (10 μM) and MMACHC-R161Q (10 μM), in the presence and in the absence of cobalamin (20 μM) and with the addition of betaine 0.5 M, with a heating rate of 0.5 °C/min, path length 1 mm, band width 3 nm, data pitch 1 min, response 16 s.

MMACHC-R161Q ellipticities at 222 nm were fitted according to the single-transition unfolding model. Under equilibrium F ⇄ U, at any temperature T the conformational equilibrium constant K is:

$$K(T) = \frac{X_F}{X_U} \tag{6}$$

where X_F and X_U are the molar fractions of folded and unfolded molecules, respectively.

and the free energy of unfolding ΔG is:

$$\Delta G(T) = -RT\ln K(T) \tag{7}$$

where the superscript for the standard Gibbs energy has been removed for the sake of clarity.

The temperature dependence of the Gibbs energy is given by:

$$\begin{aligned} \Delta G(T) &= \Delta H(T_m)\left(1 - \frac{T}{T_m}\right) + \Delta C_P\left(T - T_m - T\ln\frac{T}{T_m}\right) \\ K(T) &= exp\left(-\frac{\Delta G(T)}{RT}\right) \\ X_F(T) &= \frac{1}{1+K(T)}, X_U(T) = \frac{K(T)}{1+K(T)} \end{aligned} \tag{8}$$

where T_m is the temperature corresponding to denaturation midpoint (at which $X_F = X_U$).

The observed spectroscopic signal (S) is given by:

$$S(T) = S_F(T)X_F(T) + S_U(T)X_U(T) \tag{9}$$

where S_F and S_U correspond, respectively, to the signal arising from a protein solution of the same concentration that would contain only folded or only unfolded molecules, and they are considered to be linear functions of the temperature [23].

MMACHC-WT ellipticities at 222 nm were analyzed using the two-transition unfolding model, assuming a single intermediate state (I). The corresponding equations can be derived similarly to those for the single-transition by combining equations equivalent to Eqs. (6)–(9), considering that there are three coexisting species in equilibrium (F ⇄ I ⇄ U) and two conformational equilibrium constants K_1 and K_2 governing each transition (F ⇄ I and I ⇄ U):

$$\begin{aligned} \Delta G_i(T) &= \Delta H_{mi}\left(1 - \frac{T}{T_{m,i}}\right) + \Delta C_{P,i}\left(T - T_{m,i} - T\ln\frac{T}{T_{m,i}}\right) \\ K_i(T) &= exp\left(-\frac{\Delta G_i(T)}{RT}\right) \\ X_F(T) &= \frac{1}{1+K_1(T)+K_1(T)K_2(T)}, X_I(T) = \frac{K_1(T)}{1+K_1(T)+K_1(T)K_2(T)}, X_U(T) = \frac{K_1(T)K_2(T)}{1+K_1(T)+K_1(T)K_2(T)} \end{aligned} \tag{10}$$

and the observed spectroscopic signal (S) is given by:

$$S(T) = S_F(T)X_F(T) + S_I(T)X_I(T) + S_U(T)X_U(T) \quad (11)$$

where S_F, S_I, and S_U correspond, respectively, to the intrinsic signals for the folded molecules, partially folded molecules (intermediate state), and unfolded molecules, and they are considered to be linear functions of the temperature.

2.5. Isothermal titration calorimetry (ITC)

The interaction between MMACHC-WT or MMACHC-R161Q and ligands was assessed by isothermal titration calorimetry using a high precision Auto-iTC200 calorimeter (MicroCal, Malvern-Panalytical). Protein and ligands were separately dissolved in 20 mM PB, pH 7.4, 300 mM NaCl, 5 % *v*/v glycerol. Compounds were titrated into protein solution by performing 19 injections of 2 μL each, and mixed using a stirring speed of 750 rpm, maintaining a spacing between injections of 150 s, and applying a reference power of 10 μcal/s.

As concerns AdoCbl titration, 200 μM of AdoCbl were titrated into a solution of 10 μM MMACHC-WT or MMACHC-R161Q. The experiments were performed at 25 °C.

With regard to the titration of GSH, 500 μM of GSH were titrated into a solution of 10 μM MMACHC-WT or MMACHC-R161Q in the absence and in the presence of 20 μM AdoCbl. The experiments were performed at 25 °C and at 15 °C.

A model with a single ligand binding site was employed for data analysis. Briefly, the concentration of ligand and protein inside the calorimetric cell after each injection *j* are calculated as follows:

$$[L]_{T,j} = [L]_{syr}\left(1 - \prod_{k=1}^{j}\left(1 - \frac{v_k}{V_0}\right)\right) \quad [P]_{T,j} = [P]_{cell}\prod_{k=1}^{j}\left(1 - \frac{v_k}{V_0}\right) \quad (12)$$

where $[L]_{syr}$ is the concentration of ligand in the syringe, $[P]_{cell}$ is the initial concentration of protein in the cell, v_k is the volume of each injection, V_0 is the cell volume, and *j* is the injection number. Normally, a factor *n* multiplying $[P]_{cell}$ is included in Eq. 12 to account for a fraction of non-binding-competent protein in the calorimetric cell. The binding isotherm (ligand-normalized injection heats as a function of the molar ratio) was built by integrating the injection heat effects recorded in the thermogram (thermal power as a function of time) and the theoretical heat effect was calculated as follows:

$$Q_j = \frac{1}{v_j[L]_{syr}}V_0\Delta H\left([PL]_j - [PL]_{j-1}\left(1 - \frac{v_j}{V_0}\right)\right) + Q_d \quad (13)$$

where $[PL]_j$ is the concentration of complex formed after injection *j* and Q_d is the background injection heat (usually called "dilution heat", but it includes many other unspecific phenomena such as mechanical mixing and buffer neutralization). The concentration of complex after each injection was calculated using the following expression:

$$[PL] = \frac{1 + K_a[P]_T + K_a[L]_T - \sqrt{\left(1 + K_a[P]_T + K_a[L]_T\right)^2 - 4K_a^2[P]_T[L]_T}}{2K_a} \quad (14)$$

The equilibrium association constant, K_a, the binding enthalpy, ΔH, and the binding stoichiometry, *n*, were estimated through non-linear least squares regression analysis of the data in Origin 7.0 (OriginLab) [24].

2.6. Molecular dynamics (MD)

The coordinates of the MMACHC-WT were extracted from the pdb file 3SBZ, resulting from the crystal structure of Apo-MMACHC (1–244) [12]. The model included three malonate ions that were kept. The input was generated using the module "Solution Builder" on CHARMM-GUI, using ParamChem NSF service to parametrize the malonate ions. The protein was solvated adding water molecules such that there is a minimum distance of 1.0 nm between the simulation box walls and the closest protein atom (model TIP3P). Sodium and chloride ions were added to ensure charge neutrality. The simulations were performed using GROMACS 2023.1 [25] with periodic boundary conditions. CHARMM-36 was used as force field [26]. All bonds involving hydrogen atoms and all the water molecules are rigid.

The system potential energy was firstly minimized, and then the system was equilibrated for 2.5 ns keeping the protein and the ligand fixed harmonically restrained in the NVT ensemble at 303.15 K. The productions simulations were performed in the NPT ensemble, using a Nose-Hoover temperature coupling and a Parrinello-Rahman pressure coupling. Ten parallel simulations for a total length of 300 × 10 ns were run to enhance the sampling, and the last simulation was extended to 1 μs.

The configuration at $t = 1$ μs was used to perform a 40 ns simulation increasing the temperature from 303.15 K to 343.15 K at a constant rate. After 100 ns of simulation at 343.15 K, the temperature was further increased to 383.15 K in 40 ns as described above and then 1 μs of simulation was run. The stepwise increase in temperature allowed us to monitor the degree of disorder at different temperatures.

To model the MMACHC-R161Q, Arg-161 was changed to Gln using the rotamers tool in UCSF ChimeraX 1.5. The simulation of the mutant was run under the same conditions as the wild type.

The analysis of the resulting trajectories was performed using VMD 1.9.4 [27], UCSF ChimeraX 1.5 [28] and the python library MDAnalysis [29].

2.7. Native gel electrophoresis

Blue native-PAGE was performed with 12 μM protein (MMACHC-WTor MMACHC-R161Q) in the absence or in the presence of 120 μM AdoCbl and/or 4 mM GSH, which were loaded onto the native-PAGE gel system (4–16 % Bis-Tris 1.0 mm), after preincubation in the dark at room temperature for 1 h. The run was carried out in Dark Blue Cathode Buffer at 150 V for 40 min at 4 °C. After removing the Dark Blue Cathode Buffer, the run was completed using Light Blue Cathode Buffer at 250 V for 60 min at 4 °C. Gel was stained with InstantBlue™ and scanned on LiCor Odyssey Imaging System 9120. Blue native-PAGE experiments were performed five times independently. Densitometric analysis of the bands was performed using the Odyssey v 3.0 software.

2.8. Size exclusion chromatography (SEC)

Analytical gel filtration was performed using Superdex 200 Increase 10/300 GL (Cytiva) pre-equilibrated with 20 mM PB pH 7.4, 300 mM NaCl, 5 % *v*/v glycerol, on a modular Prominance Shimadzu HPLC device, equipped with a mobile phase degasser (DGSU-20As), a quaternary pump (LC-2010 AT) and a photodiode array detector (SPD-M20A). MMACHC-WT or MMACHC-R161Q (15 μM) were incubated for 10 min at room temperature with AdoCbl in a molar ratio 1:10 and eluted with the same buffer.

2.9. Static and dynamic light scattering (SLS and DLS)

The samples, freshly prepared and filtered using 0.2 μm Millex-GV filters (45 μM MMACHC-WT or MMACHC-R161Q in the absence and in the presence of a 2-fold molar excess of AdoCbl) were placed into a dust-free quartz cell and kept at 20 °C in the thermostated cell compartment of a Brookhaven Instruments BI200-SM goniometer. The temperature was controlled within 0.1 °C using a thermostated recirculating bath. Light scattering experiments were carried directly filtered samples in a quartz cylindrical cuvette (0.2 μm LG Millex filter). Measurements were performed on a Brookhaven Instrument BI-9000

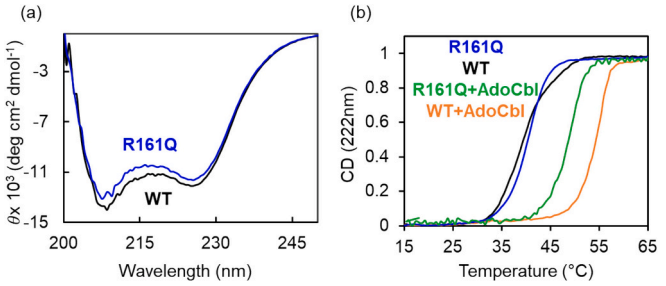

Fig. 1. (a) CD spectra of MMACHC-WT and MMACHC-R161Q (b) Thermal denaturation curves of MMACHC-WT and MMACHC-R161Q obtained by measuring the ellipticity at 222 nm as a function of temperature in presence and in the absence of AdoCbl. The ellipticity values have been normalized for appropriate comparison.

Table 1
Unfolding temperatures resulting from the fitting of the CD thermal denaturation data with two-state model, in the case of MMACHC-R161Q mutant, and three states in the case of MMACHC-WT protein.

		−Cbl	+Cbl
WT	T_{m1}	38.5 ± 0.1 °C	52.2 ± 0.1 °C
	T_{m2}	46.9 ± 0.1 °C	56.1 ± 0.1 °C
R161Q	T_m	40.2 ± 0.2 °C	45.8 ± 0.1 °C

goniometer, equipped with a 20 mW He—Ne laser with wavelength.

$\lambda_0 = 632.8$ nm. The intensity of the scattered light, I(t), and the intensity autocorrelation function, $g_2(t)$, were measured simultaneously by using the Brookhaven BI-9000 correlator. Measurements were taken at the angle $\theta = 90°$, corresponding to a scattering vector $q = \frac{4\pi n}{\lambda_0}\sin\frac{\theta}{2} = 18.7\ \mu m^{-1}$, where n is the refractive index of the solution and λ_0 is the in vacuo laser wavelength. The field autocorrelation function $g_1(t) = \sqrt{(g_2(t)-1)}$, was obtained from the measured $g_2(t)$, and analyzed by using an inverse Laplace transform by means of a constrained regularization algorithm (CONTIN) [30], in order to determine the distribution $A(\Gamma)$ according to:

$$g_1(t) = \int A(\Gamma)e^{-\Gamma t}d\Gamma \tag{15}$$

where $A(\Gamma)$ represents the contribution to the $g_1(t)$ amplitude, due to the species with diffusion coefficient D, considering the decay rate $\Gamma = Dq^2$. Then, by applying the Stokes−Einstein relation.

$R_h = \frac{k_B T}{6\pi\eta D}$ (where k_B is the Boltzmann constant, T the absolute temperature and η the solvent viscosity), the distribution function of the decay rates is converted into the intensity-weighted hydrodynamic radius distribution $A(R_h)$, from which mean hydrodynamic radius is obtained.

From the static light scattering intensity monitored every second, the average molar mass M_w values were calculated according the following relation

$$I_{90^\circ} \propto kM_w cP\ (\theta = 90^\circ) \tag{16}$$

with c the protein concentration and $k = \frac{4\pi^2 n^2}{\lambda_0^4 N_A \left(\frac{dn}{dc}\right)^2}$, where N_A is the Avogadro number [31], and we considered the form factor $P \sim 1$ and $dn/dc = 0.18\ cm^3 g^{-1}$.

2.10. Small angle X-ray scattering (SAXS)

SAXS measurements were performed at the Austrian beamline of the Elettra Synchrotron in Trieste, Italy. Scattering patterns were acquired using a Pilatus3 X 1 M detector system (Dectris, Switzerland), while a photodiode on the beamstop monitored the transmitted X-ray beam. All experiments were carried out at a constant temperature of 10 °C. The 2D detector images were radially averaged to obtain the scattering intensity as a function of the scattering vector magnitude, Q, defined as $Q = \frac{4\pi \sin\theta}{\lambda}$, where 2θ is the scattering angle and λ = 0.154 nm is the X-ray wavelength. Data corrections were applied for sample transmission and primary beam fluctuations.

For each sample, individual scattering patterns were averaged along with their corresponding background signals. Background SAXS spectra were subtracted from the sample SAXS patterns. The μ-Drop sample changer, specifically developed for the Austrian beamline [32], was used for our experimental set-up. Each measurement was performed on 15 μL sample volumes for 20 s, repeated at least four times with a 5 s interval between each acquisition. To enhance the signal-to-noise ratio, a minimum of four sample injections were carried out. Buffer measurements were systematically conducted before and after sample acquisitions. SAXS curves were obtained for both MMACHC-WT and MMACHC-R161Q at a concentration of 263 μM. SAXS curves were analyzed applying the Guinier law: $I(Q) = I(0)e^{-\frac{R_g^2 Q^2}{3}}$, where I(0) is the scattering intensity at $Q = 0$ and R_g is the gyration radius of the scattering particles, which provides an estimation of the overall size of the particles in solution.

2.11. Isothermal denaturation (ITD)

MMACHC-WT and MMACHC-R161Q were diluted to 0.1 mg/mL (3 μM) in buffer containing 20 mM PB pH 7.4, 300 mM NaCl, 5 % *v*/v glycerol with 1:1000 SYPRO Orange (Invitrogen) and 0.5 M of different osmolytes (betaine, proline, arginine, trehalose). Samples of both proteins were kept at a constant temperature of 38 °C while the fluorescence of the probe was monitored by a Fluoroskan™ FL Microplate Fluorometer, equipped with 485 nm excitation and 538 nm emission filters.

2.12. Dealkylation assay

Dealkylation activity was monitored as previously described [14] with minor modifications. A solution containing 16 μM protein was incubated with 12.8 μM MeCbl in the absence or presence of 0.5 M of betaine for 10 min at room temperature. The reaction was started by the addition of 1 mM GSH. Spectra were recorded using a SHIMADZU UV-VIS Spectrophotometer at 20 °C. The time dependence of dealkylation activity was monitored following the increasing absorption at 353 nm in time. Data were expressed as the increase in absorbance at 353 nm normalized to the initial value, as follows (Abs_{353nm}(t)–Abs_{350nm} (t_0))/ Abs_{350nm} (t_0), where t_0 represent the time of GSH addition. The data were analyzed by interpolating experimental points with a single exponential fit of the form $y = y_0 + a(1 - \exp(-bt))$. The observed dealkylation rate constants k_{obs} were determined from the fit as the slope of tangent line to experimental curves at $t = 0$.

3. Results

3.1. Impact of R161Q mutation on MMACHC stability

Our first objective was to investigate the structural and stability properties of the MMACHC-R161Q mutant to understand whether it could be representative of pathological mutations that affect the folding and stability of MMACHC, making it potentially susceptible to correction by folding rescuers. First, we predicted the protein stability changes induced by the substitution R161Q, along with the most common point mutations found in cblC, using PremPS, a computational method that evaluates the difference in folding Gibbs energy resulting from the substitution of the involved residue with alanine [33]. Based on the free

Table 2
Thermodynamic parameters resulting from the analysis of the DSC thermal unfolding thermograms for MMACHC-WT and MMACHC-R161Q.

	T_{m1}(°C)	ΔH_{m1} (kcal/mol)	T_{m2} (°C)	ΔH_{m2} (kcal/mol)
WT	39.2 ± 0.1	96 ± 2	48.6 ± 0.1	97 ± 2
R161Q	39.3 ± 0.1	109 ± 2	42.1 ± 0.1	65 ± 2

Table 3
Mode of the molecular mass distribution from MMACHC-WT and MMACHC-R161Q in the presence and in the absence of AdoCbl.

	Mode of the molecular mass distribution (kDa)	Mode channel percentage (%)
WT	46.70 ± 0.08	93
WT + AdoCbl	58.09 ± 0.06	91
R161Q	41.75 ± 0.06	100
R161Q + AdoCbl	43.1 ± 0.1	94

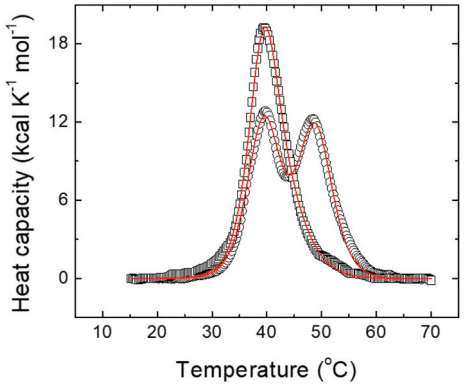

Fig. 2. DSC thermograms of apo MMACHC-WT (circles) and MMACHC-R161Q (squares) proteins. The experimental data (empty symbols) and the theoretical fit of the data to a two-transition model (continuous lines) for both proteins are shown.

energy variation values (ΔΔG), R161Q and other point mutations were found to have a destabilizing effect on the protein (Supporting Information, Table S1).

We confirmed this result by studying the structure and stability of the recombinant MMACHC-R161Q, which was purified following the protocol we previously developed for the MMACHC-WT protein [21,34]. We initiated our investigation by examining MMACHC-R161Q structure by CD in the FAR-UV region. The resulting CD spectrum revealed minimal changes compared to the spectrum of the wild-type protein (Fig. 1a) and both the proteins exhibit a secondary structure predominantly composed of alpha-helix elements, as evidenced by characteristic minima at 208 and 222 nm in the CD spectrum.

However, the thermal unfolding profile of MMACHC-R161Q, obtained by monitoring ellipticity as a function of temperature, revealed a markedly different behavior from that of MMACHC-WT, both in the presence and in the absence of AdoCbl. In fact, although at first sight the unfolding of the two apoproteins showed minor differences in unfolding temperatures, their shape is appreciably different (Fig. 1b). The unfolding profile of the wild type protein reveals the presence of two transitions as also suggested by Froese et al. [15], and it could be fitted only using a two-transition model. On the other hand, the MMACHC-R161Q mutant CD thermal unfolding could be analyzed by using a single transition model.

In Table 1 the unfolding temperatures obtained for the two wild-type

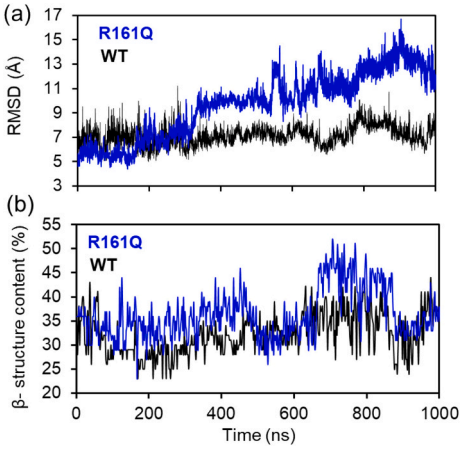

Fig. 4. MD characterization of MMACHC-WT and MACHC-R161Q thermal unfolding intermediate. Root-mean-square deviations (RMSD) (a) and beta structure content (b) from wild type and mutant structure along 1 μs of simulation carried out after two temperature jumps, 40 K each, from 303.15 K.

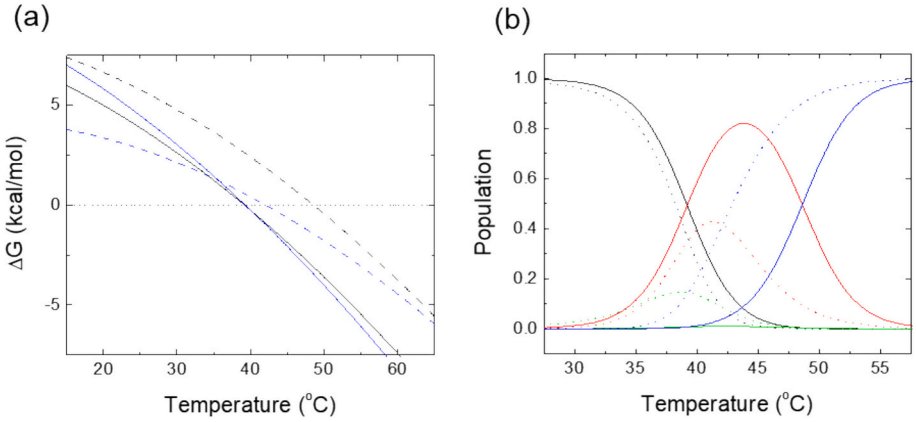

Fig. 3. (a) Stability Gibbs energy of the less stable domain ΔG_1 for MMACHC-WT (black, continuous line) and for MMACHC-R161Q (blue, continuous line), and stability Gibbs energy of the more stable domain ΔG_2 for MMACHC-WT (black, dashed line) and for MMACHC R161Q (blue, dashed line). (b) Temperature dependence of the populations of the different conformational states for MMACHC-WT (continuous lines) and MMACHC-R161Q (dotted lines): folded state (black), first intermediate state (red), second intermediate state (green), and unfolded state (blue). The conformational landscape for the wild type protein comprises three significantly populated conformational states, whereas the conformational landscape of the mutant protein comprises four significantly populated states. (For interpretation of the references to colour in this figure legend, the reader is referred to the web version of this article.)

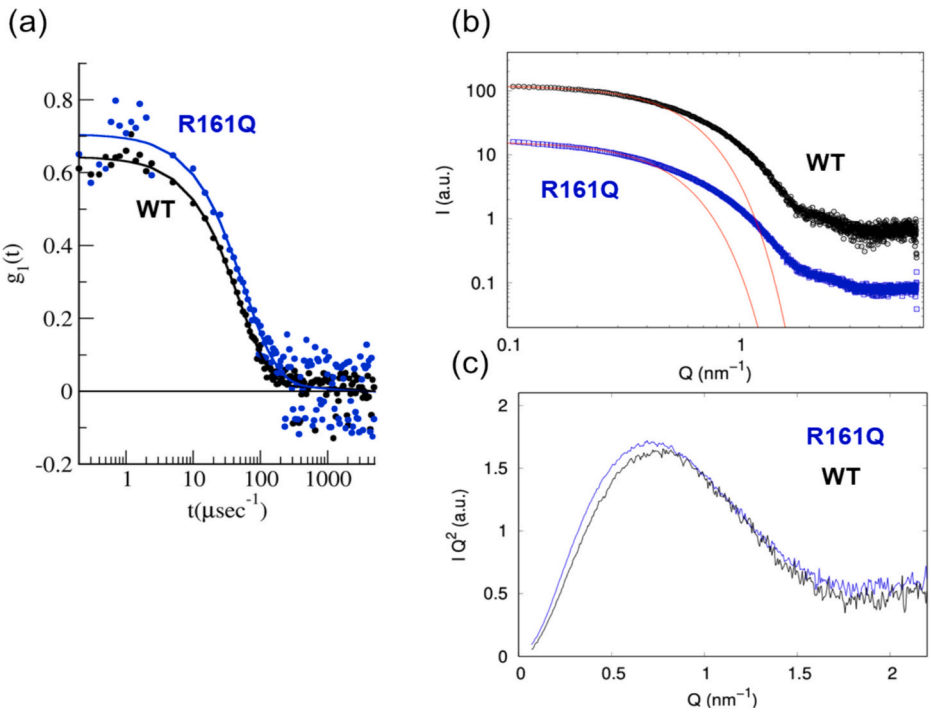

Fig. 5. (a) First-order autocorrelation functions $g_1(\tau)$ obtained from dynamic light scattering experiments carried out on MMACHC-WT and MMACHC-R161Q proteins. Continuous lines represent fitting curves obtained by applying constrained regularization analysis through the CONTIN algorithm, based on the inverse Laplace transform (b) SAXS curves for MMACHC-WT and MMACHC-R161Q, vertically offset for clarity. Red continuous lines indicate Guinier approximation fits (c) Kratky plots derived from the SAXS data. (For interpretation of the references to colour in this figure legend, the reader is referred to the web version of this article.)

protein transitions and the single mutant transition are reported both in the presence and in the absence of AdoCbl. As shown in Table 1, the unfolding temperature changes substantially in the presence of AdoCbl both for wild type and for the mutant. Moreover, it appears that the less stable domain of MMACHC is more significantly influenced by the binding of AdoCbl. The presence of two transitions in the thermal denaturation of MMACHC-WT protein becomes quite evident from the thermograms resulting from DSC experiments.

Also in this case, the wild-type protein data could not be analyzed considering a single transition model, but an additional transition needs to be added to reproduce the experimental data. However, very interestingly, also the DSC curve for the MMACHC-R161Q mutant had to be analyzed by assuming the presence of two transitions, thus, considering low populated intermediate conformations. The thermodynamic parameters obtained from the calorimetric analysis for both proteins are reported in Table 2. While the unfolding temperature of the first transition, T_{m1}, is the almost the same for the two proteins, the second unfolding temperature, T_{m2}, for the mutant is significantly lower with respect to wild-type, and close to T_{m1}. Hence, in the case of MMACHC-R161Q the two transitions overlap considerably giving rise to a single broader peak which can be apparently associated to a single transition. This also explains why the CD assay showed a single apparent transition, which could not be fitted with two distinct transitions due to degeneracy or convergence issues in the fitting procedure.

Since the unfolding enthalpy and the unfolding temperature of the first transition are similar for both proteins, the stabilization energy gap between the folded state and the first intermediate state are comparable (Fig. 3a). However, the lower unfolding enthalpy and unfolding temperature for the second transition in the mutant implies that the main intermediate conformational state for the mutant is either less stable or structurally different from that of the wild type, possibly leading to a more destabilized overall folding pathway. This can be observed when calculating the populations of the different states as a function of temperature for MMACHC-WT and MMACHC-R161Q (Fig. 3b), according to Eq. 5 and the stability parameters obtained from the DSC assays. In the case of MMACHC-WT, the first intermediate reaches a maximal population of 0.82 at 43.8 °C, but the second intermediate is barely populated with a maximal population of 0.009 at 42.3 °C, resulting in an "effective" three-state scenario. However, in the case of MMACHC-R161Q, the first intermediate has a much lower presence with a maximal population of 0.43 at 41.3 °C, but the second intermediate has a non-negligible role with a maximal population of 0.15 at 38.7 °C, resulting in an "effective" four-state scenario.

To better understand the impact of the R161Q mutation on the thermal unfolding process of the protein, we conducted molecular dynamics (MD) simulations. Specifically, the temperature of the MMACHC-WT and MMACHC-R161Q systems was increased in two steps of 40 K each, starting from 303.15 K, with heating ramps lasting 40 ns each. It is important to note that temperature increases in MD simulations do not directly correspond to real experimental conditions [35]. Due to the limited timescales accessible in MD, elevated temperatures are commonly used to accelerate unfolding events and enhance sampling, rather than to replicate physiological temperature changes. Thus, the observed effects should be interpreted in the context of comparative dynamics under controlled, yet artificial, thermal stress conditions. Because no relevant structural changes were detected in either protein after the first 40 K ramp, we performed a second ramp and then ran a 1 μs simulation. The results revealed that, while the root-mean-square deviation (RMSD) of the wild-type protein — calculated with respect to its most stable region (the N-terminal α-helix and the adjacent β-sheet strand) — remained below 10 Å, the R161Q mutant showed progressively higher RMSD values, peaking at 15 Å (Fig. 4a). This indicates that, after the two 40 K jumps, the mutant loses a significant portion of its tertiary structure, whereas the wild-type protein remains stable.

This also suggests that the simulated thermal jumps do not correspond to a complete unfolding leading to protein full denaturation, but rather to the attainment of an unfolding intermediate state. The secondary structure of the R161Q mutant differed from the wild type solely by a minor increase in small β-strands (Fig. 4b).

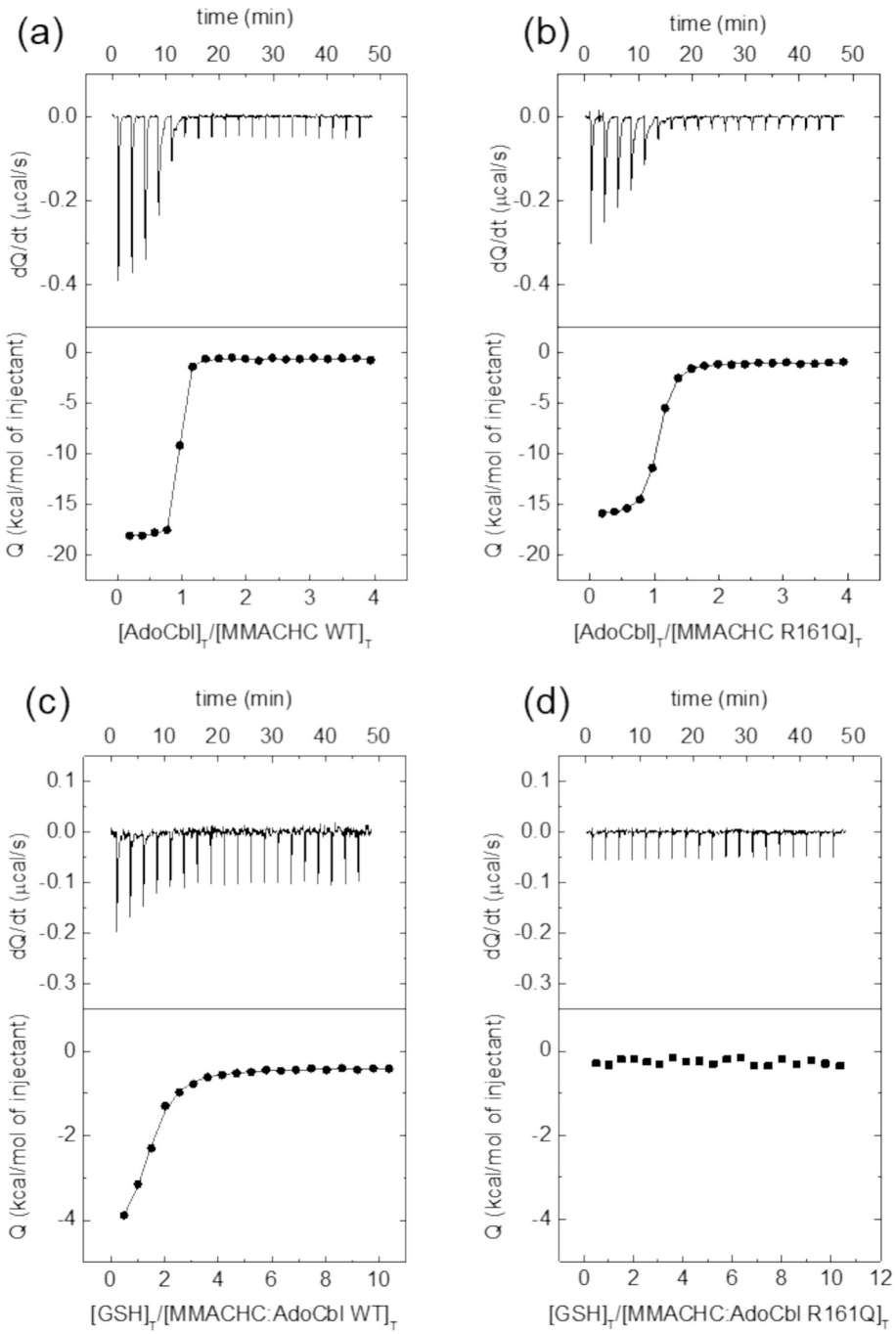

Fig. 6. Calorimetric titrations for MMACHC-WT interacting with AdoCbl (a) and GSH (c), and MMACHC-R161Q interacting with AdoCbl (b) and GSH (d). The titrations with GSH were performed in the presence of AdoCbl, prebound to the protein in the calorimetric cell. The upper plots provide the thermograms, while the lower plots display the binding isotherms fitted to a single binding site model.

3.2. Structural effects of the R161Q mutation on MMACHC apoprotein

To elucidate the structural differences between the two proteins, we performed analyses on their apo forms using Dynamic Light Scattering (DLS) and Small-Angle X-ray Scattering (SAXS). The electric field autocorrelation functions, $g_1(\tau)$, obtained from DLS measurements of apo MMACHC-WT and apo MMACHC-R161Q, revealed distinct decay profiles, indicating differences in their diffusion motions (Fig. 5a). The average hydrodynamic radius (R_h) from these measurements showed that apo MMACHC-WT (R_h = 3.6 nm) was approximately 12 % smaller than the mutant apo MMACHC-R161Q (R_h = 4.1 nm). A similar size ratio was observed from the radius of gyration (R_g) values derived through Guinier analysis of SAXS data, with MMACHC-WT exhibiting an R_g of 3.2 nm compared to 3.7 nm for MMACHC-R161Q (Fig. 5b).

These size discrepancies between wild type and mutant proteins could reflect either a more open and loose conformation and/or an increased propensity for aggregation in the mutant form, both indicative of potential differences in conformational stability. Moreover, the Kratky plots from SAXS measurements further supported these hypotheses, as the bell shape of the plot corresponding to the mutant protein is centered at lower *Q* values, in agreement with a wider gyration radius. Also, an higher wideness of Kratky plot corresponding to the mutant is consistent with a higher flexibility and reduced structural compactness (Fig. 5c).

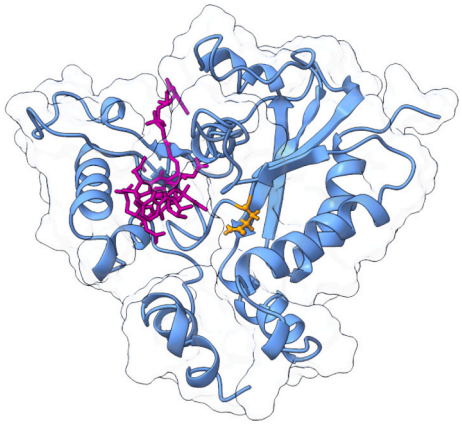

Fig. 7. Structure of MMACHC-R16Q mutant, obtained by substituting the Arg-161 residue with Gln in the pdb file 5UOS, using UCSF ChimeraX 1.5. The mutated residue and base-off AdoCbl are both represented as sticks and colored yellow and magenta, respectively. (For interpretation of the references to colour in this figure legend, the reader is referred to the web version of this article.)

3.3. Impact of mutation R161Q on MMACHC binding to substrates

As previously discussed, the thermal unfolding analysis of MMACHC-WT and MMACHC-R161Q proteins revealed that the ligand-induced stability increase for the mutant is considerably smaller than that observed for the wild type. When previously assessed by differential scanning fluorimetry, this difference in stabilization was considered indicative of the lower affinity shown by the MMACHC-R161Q to the AdoCbl with respect to MMACHC-WT [15]. However, to our knowledge, no direct experiment has ever been performed aimed to quantitatively assess the binding of AdoCbl to MMACHC-WT, or to its pathological mutants. We previously compared the binding of MMACHC-WT to AdoCbl with the MMACHC-R132X protein resulting from the nonsense c.394C > T pathological mutation of MMACHC by assessing the progressive quenching in proteins intrinsic fluorescence at increasing AdoCbl concentrations. However, while this method allowed us and others [21,36] to obtain important comparative information across different conditions, it might provide only apparent affinity values that are not necessarily reliable in absolute terms. Therefore, we used isothermal titration calorimetry (ITC) to obtain quantitative information on binding, as this technique is considered nowadays the gold standard for binding affinity determination in biomolecular interactions [37]. From the analysis of the data using a single binding-site model, we observed that the affinity of MMACHC-WT for AdoCbl ($K_d = 15 \pm 2$ nM) was significantly higher than that of MMACHC-R161Q ($K_d = 104 \pm 8$ nM). The interaction of AdoCbl is enthalpically driven in both cases: the binding enthalpy is −17.6 kcal/mol and − 15.2 kcal/mol for MMACHC-WT and MMACHC-R161Q, respectively (Fig. 6). The 7-fold reduction in AdoCbl affinity for the mutant protein ($\Delta\Delta G = 1.2$ kcal/mol) with respect to the wild-type protein is the result of a less favorable enthalpy

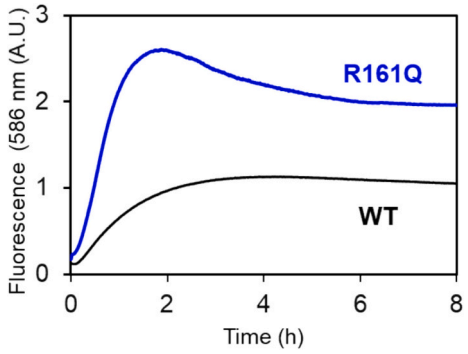

Fig. 9. Time dependence of SYPRO Orange fluorescence emission at 490 nm upon excitation at 490 nm at the fixed temperature of 38 °C incubated with MMACHC-WT and MMACHC-R161Q mutant.

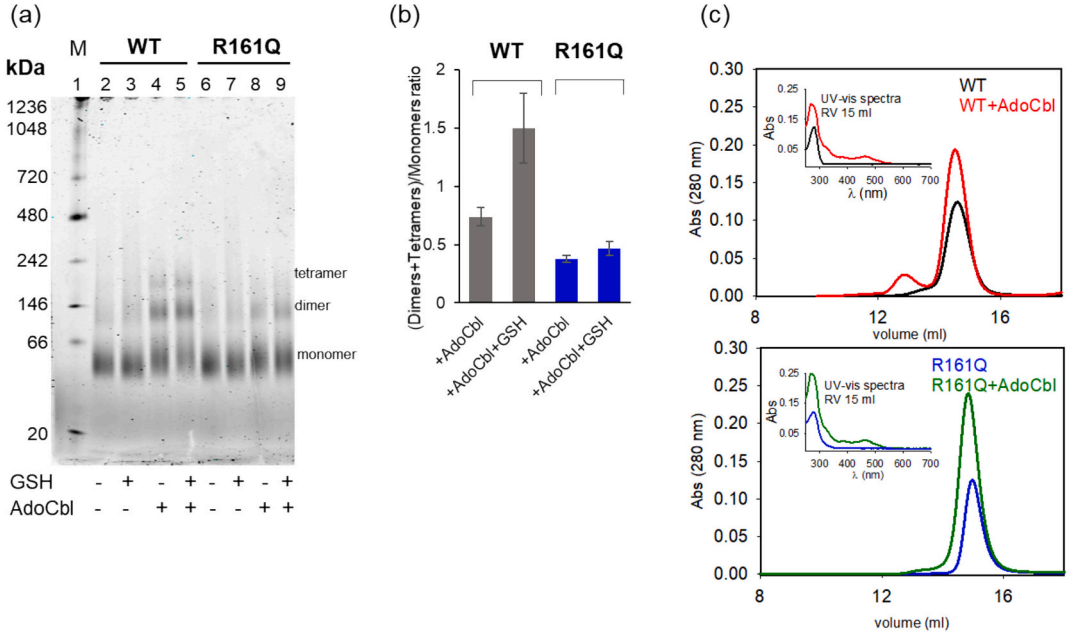

Fig. 8. Oligomeric state analysis of MMACHC-WT and MMACHC-R161Q mutant. (a) Representative BN-PAGE gel showing: MMACHC-WT or MMACHC-R161Q mutant protein in the absence (lanes 2 and 6) or presence of AdoCbl (lanes 4 and 8), or in the presence of GSH (lanes 3 and 7), or in the presence of GSH + AdoCbl (lanes 5 and 9). M, protein marker (line 1). (b) (Dimers+Tetramers)/Monomers ratio obtained from the densitometric analysis of the BN-PAGE band intensities and performed by using Odyssey 3.0 software. Data are expressed as the mean ± SD of five independent experiments. (c) Chromatographic profile of MMACHC WT and MMACHC R161Q mutant in the absence and in the presence of AdoCbl. In the insets the corresponding absorbance spectra relative to 15 mL retention volume (RV) are reported.

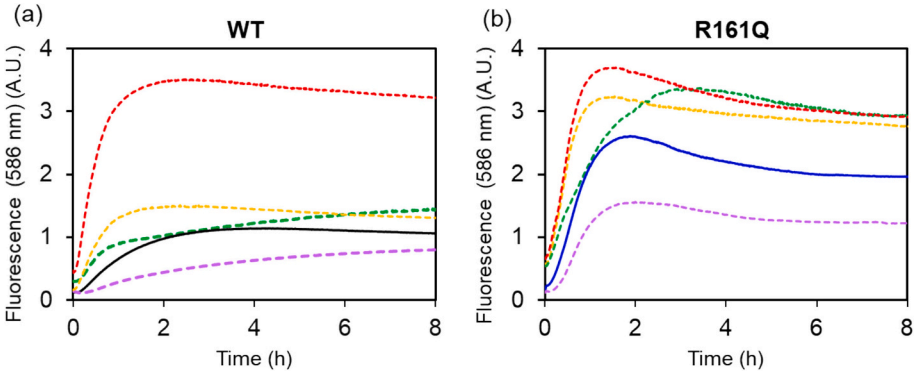

Fig. 10. Time dependence of SYPRO Orange fluorescence emission at 586 nm upon excitation at 490 nm at of 38 °C incubated with MMACHC-WT (a) and MMACHC-R161Q mutant (b) in the absence (continuous black for wild type and continuous blue for R161Q mutant) and in the presence of several chemical chaperones (CCs): arginine (dashed red), proline (dashed yellow), trehalose (dashed green), betaine (dashed purple). (For interpretation of the references to colour in this figure legend, the reader is referred to the web version of this article.)

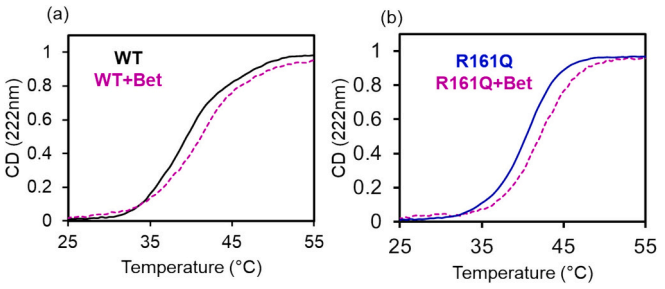

Fig. 11. Thermal unfolding curves obtained by monitoring ellipticity at 222 nm as a function of the temperature for MMACHC-WT (a) and MMACHC-R161Q mutant (b) in the absence and in the presence of 0.5 M of betaine. The ellipticity values have been normalized for appropriate comparison.

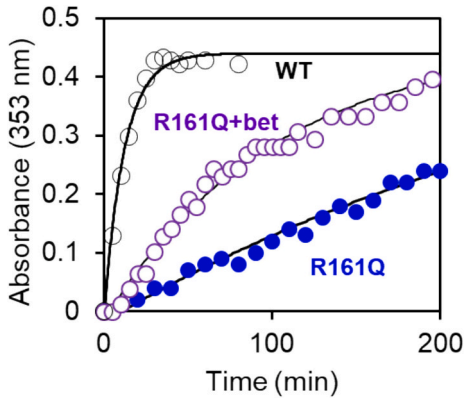

Fig. 12. Dealkylation activities assessed by monitoring the time evolution of the absorbance at 353 nm of MeCbl incubated with MMACHC proteins after GSH addition. Data are expressed as the increase in absorbance at 353 nm normalized to the initial value. Continuous lines represent single-exponential fits to the experimental data obtained for MMACHC-WT, and MMACHC-R161Q in the presence and absence of betaine.

($\Delta\Delta H = 2.4$ kcal/mol) and a more favorable entropic contribution to the binding Gibbs energy ($-T\Delta\Delta S = -1.2$ kcal/mol).

We conclude that the altered folding and stability properties shown by the MMACHCR161Q mutant also affect the structural properties of the MMACHC Cblbinding pocket, even though the mutated residue lies outside that region (Fig.7).

Concerning the binding to glutathione (GSH), the required cofactor for protein dealkylation activity, the calorimetric experiments showed that no binding could be detected between the tripeptide and apo-MMACHC for both proteins (Fig. S1 Supplementary Materials). After verifying by absorption spectroscopy that the dealkylation rate of AdoCbl in the presence of MMACHC WT with GSH was sufficiently slow to avoid significant changes in AdoCbl during the ITC experiment (lasting approximately 1 h, Fig. S2 Supplementary Materials), we performed ITC measurements by titrating GSH into a solution of the binary complexes AdoCbl–MMACHC WT or AdoCbl–MMACHC R161Q. We found that while GSH was observed to interact with the complex AdoCbl-MMACHC-WT with $K_d = 2.1 \pm 0.2$ μM, no interaction could be detected between GSH and the complex AdoCbl-MMACHC-R161Q.

Two important points follow from these ITC data: first, the structural rearrangements induced by Cbl binding to MMACHC [21] are necessary for glutathione subsequent binding. Second, these structural rearrangements induced by Cbl binding in MMACHC-R161Q do not guarantee the binding of the GSH to the protein. This is not surprising considering that arginine at position 161 is one of the residues involved in the tripeptide binding [13,38]. However, we cannot exclude that the binding to glutathione is affected by the folding defects triggered by the mutation on the protein.

3.4. Impact of mutation R161Q on protein oligomeric organization

Since we found that the R161Q mutation induces variations in the global folding of MMACHC and its Cbl-binding region, our next aim was to understand its role in the formation of MMACHC dimers, supposed to result from domain swapping involving the two Cbl moieties in the MMACHC subunits [13]. We assessed the assembly of the wild-type protein and R161Q mutant by using several methodologies. First, we studied MMACHC-WT and MMACHC-R161Q oligomeric state in the absence and in the presence of AdoCbl, GSH and AdoCbl+GSH by using Blue Native-PAGE, a technique that separates multiprotein complex in a native conformation. A representative gel of five independent experiments is reported in Fig.8a (the other four gels are reported in Fig. S3, Supplementary Materials). This gel shows that both wild-type and R161Q mutant proteins predominantly exist in the monomeric state in their apo form, with only a very small amount of dimers detected more prominently in the MMACHC-WT sample (Fig. 8a, lane 2 and 6). Similar results were obtained in the presence of GSH (Fig. 8a, lane 3 and 7). However, upon addition of AdoCbl, dimer formation significantly increased in the MMACHC-WT protein and in higher extent compared to the MMACHC-R161Q (Fig. 8a, lane 4 and 8). Additionally, a further increase in dimer population was observed only for the wild-type protein when GSH was added to the protein-Cbl complex (Fig. 8a, lane 5 and 9). Very interestingly, a band corresponding to a tetramer could be found in the MMACHC-WT sample in the presence of AdoCbl and

AdoCbl+GSH, suggesting the formation of more complex hierarchical structures as also found by Froese et al. [13]. Densitometric analysis of the monomeric and oligomeric forms under various conditions revealed that the dimers/tetramers-to-monomer ratio was significantly higher for the wild-type protein compared to the R161Q mutant. (Fig. 8b). We confirmed the different propensity of MMACHC-WT and MMACHC-R161Q proteins to form homodimers by using SEC. In both cases, when incubated with the proteins, AdoCbl exhibits an absorption peak at 460 nm, reflecting the conformational base-off state achieved by vitamin B12 upon binding to the proteins (insets, Fig. 8c) [21].

The chromatographic profile of the MMACHC-WT protein in the presence of AdoCbl revealed a distinct peak corresponding to its dimeric structure, whereas the MMACHC-R161Q mutant displayed only a shoulder at the same position (Fig. 8c). Quantitative analysis of the peak areas corresponding to the monomeric and dimeric species indicated that, in the absence of ligands, ~6 % of dimers were formed exclusively in the apo wild-type protein, while no dimers were detected in the apo R161Q mutant. Upon addition of AdoCbl, the dimer-to-monomer ratio increased to 0.5 in the MMACHC-WT sample, whereas it remained very low (0.03) in the R161Q mutant.

Furthermore, we obtained information on the molecular mass of the proteins in solution using static light scattering, from which molecular mass distributions for MMACHC-WT and MMACHC-R161Q were derived. As shown in Table 3, which reports the mode of the molecular mass distributions, the most frequent molecular mass value obtained for MMACHC-WT incubated with AdoCbl is significantly higher than that observed for MMACHC-R161Q. In the absence of ligands, the slightly higher molecular mass observed for the wild-type protein may be attributed to the greater amount of dimers — although low in abundance — detected in the apo MMACHC-WT compared to the apo MMACHC-R161Q, as evidenced by native gel electrophoresis and SEC.

Overall, these results demonstrate that AdoCbl plays a critical role in dimer formation and that the R161Q mutant shows a significantly reduced ability to form homodimers compared to the WT. Although each technique has its specificities, the consistent results obtained across different methods probing the oligomeric state in various molecular milieu, allow us to draw these conclusions with high confidence.

3.5. Role of betaine on R161Q stability and function

The use of chemical chaperones (CCs), osmolytes known for their ability to stabilize the protein structure, have been suggested as a potential route for rescuing the impaired activity of pathological mutants involved in rare metabolic conformational diseases [39,40]. In the case of MMACHC-R161Q mutant, we tested betaine, proline, trehalose, and arginine. In order to perform the simultaneous screening of several compounds and assess their ability to stabilize wild-type protein and R161Q mutant, we used a high-throughput assay detecting the kinetics of unfolding by the change in fluorescence of SYPRO Orange, a hydrophobic dye which can interact with hydrophobic patches thereby increasing its fluorescence intensity, thus indirectly reporting protein unfolding [41]. In order to evaluate the unfolding behavior of the proteins in the presence of the different compounds, we used a temperature-jump isothermal denaturation procedure [42] and registered the time evolution of the dye fluorescence emission at 586 nm upon excitation at 490 nm at the fixed temperature of 38 °C.

The time dependence observed in the isothermal denaturation is a multistep process with the presence of different species, each one with a particular affinity for SYPRO orange and a particular contribution to the observed signal. Hence, the dissimilarity in the shape of the denaturation curves between MMACHC-WT and MMACHC-R161Q (Fig. 9) can be ascribed to the distinct conformational populations shown by the two proteins [42].

As a next step we performed isothermal denaturation experiments of the proteins by using SYPRO orange in the presence of arginine, proline, betaine and trehalose (Fig. 10).

We that found betaine was the most effective in reducing both the plateau and the initial slope of the denaturation curves (Fig. 10). This indicates an enhanced stabilization effect exerted by betaine on both MMACHC-WT and MMACHC-R161Q protein [42].

Betaine is already employed therapeutically in cblC disease [5], primarily as a methyl donor to convert homocysteine into methionine, thereby lowering plasma total homocysteine levels in homocystinuria patients. Our results indicate that betaine can also stabilize a MMACHC mutant associated with cblC disease, suggesting a potential chaperone-like activity.

To validate the protective effect of betaine, identified as the only effective compound in previous experiments, against MMACHC denaturation, and to exclude any bias from the extrinsic dye, we used CD spectroscopy to assess the thermal unfolding process exclusively for this osmolyte (Fig. 11). Once again, we confirmed the role of betaine in stabilizing both the wild-type protein and the R161Q mutant as also shown by the increase of unfolding temperatures induced by the presence of the osmolyte.

Hence, we wanted to understand whether betaine could also have a role in improving the dealkylation activity of MMACHC-R161Q, which was evaluated spectroscopically upon addition of GSH to a solution of protein bound to an alkylcobalamin. In fact, the removal of upper ligand leads to the formation of OH_2Cbl with the appearance of a characteristic peak at 353 nm in the Cbl absorbance spectrum. Due to the slow intrinsic dealkylation of AdoCbl [14] and the low stability of MMACHC, dealkylation activity in vitro is more conveniently measured using MeCbl as a substrate by monitoring absorption at 353 nm over time.

Under our experimental conditions, the reaction catalyzed by MMACHC-WT reaches its completion within one hour. The MMACHC-R161Q mutant does bind MeCbl, as the absorption spectrum of the latter shifted from 530 nm to 460 nm, indicating its transition from the base-on to the base-off state [14]. However, minimal changes in the Cbl absorption spectrum were observed within one hour of GSH addition (Fig. 12).

From the time dependence of the absorbance change at 353 nm, the estimated dealkylation rates k_{obs} were 0.038 ± 0.004 min^{-1} and 0.0020 ± 0.0005 min^{-1} for wild type and R161Q mutant, respectively. We conclude that, as previously assessed by Froese et al. [13], the MMACHC-R161Q mutant is significantly less efficient then MMACHC-WT in removing the MeCbl upper ligand.

Interestingly, when we repeated the dealkylation test for the MMACHC-R161Q mutant in the presence of betaine, we observed a partial recovery in protein function (Fig. 12), being the k_{obs} estimated by the absorbance variation at 354 nm 0.0066 ± 0.0007 min^{-1}. Although we did not expect a complete recovery, given that the MMACHC-R161Q function is significantly impaired by its reduced binding to GSH in addition to overall destabilization, it appears that betaine can partially restore protein functionality. This result helps to elucidate the role of structural stabilization in designing therapeutic strategies for cblC.

4. Discussion

The c.271dupA frameshift mutation in the MMACHC gene is the most prevalent genetic alteration in cblC, resulting in a significant decrease in protein expression. However, around 10 % of patients carrying this mutation on one allele also harbour a missense variant on the other. To date, approximately 20 missense mutations have been identified, some of which are linked to later-onset symptoms [2,3]. Hence, unlike c.271dupA, which dramatically reduces protein levels, these point mutations are often associated with a reduced function of the expressed protein. Investigating these variants provides key insights into the relationship between genetic mutations and protein dysfunction leading to pathology [2].

Our research focused on the effect of the most common point mutation, c.482G > A, on the structure, stability, dimerization propensity, and AdoCbl binding properties of the resulting MMACHC-R161Q

protein, proven by Gherasim et al. to be strongly impaired in the ability to catalyse the transformation of MeCbl to H_2OCbl in the presence of GSH [43]. In good agreement with these results, we found, by using absorption spectroscopy, that MMACHC-R161Q, produced as soluble protein in our laboratories, presented an estimated dealkylation rate 16-fold lower compared to MMACHC-WT (Fig. 12). We conclude that, as previously assessed [43], the R161Q mutant is significantly less efficient in removing the MeCbl upper ligand. This is not surprising since the mutation affects the arginine residue in position 161 belonging to the cluster of arginines which, through specific hydrogen bonds and ionic interactions, determines GSH binding to MMACHC [13].

Here, for the first time, the binding of glutathione to MMACHC (WT or R161Q) complexed with a form of cobalamin, was quantitatively measured using ITC. Our results show that while no binding of GSH to MMACHC-WT apoprotein was detected (Fig. S1), a micromolar affinity was observed between the tripeptide and the wild type when complexed with AdoCbl (Fig. 6c). This suggests that cobalamin induces a conformational change in MMACHC, shifting the conformational equilibrium towards a GSH binding-competent conformation, allosterically modifying the GSH binding site, and enhancing its affinity for the tripeptide. In contrast, no binding was observed between GSH and the MMACHC-R161Q mutant, neither in the absence nor in the presence of AdoCbl (Fig. 6d and Fig. S1). While the arginine-to-glutamine substitution directly disrupts local interactions with negatively charged molecules such as GSH (Fig.S4), we cannot exclude the possibility that the reduced ability to bind GSH results from an impairment of the cobalamin-induced allosteric conformational change in the R161Q mutant. In fact, when we measured the binding affinity of AdoCbl to both proteins using ITC, we found that AdoCbl displayed a 7-fold reduction in affinity for MMACHC-R161Q compared to the wild-type protein (Fig. 6 a,b). This finding supports the idea of a functional interplay between cobalamin and GSH binding, which is likely important for MMACHC's role in vitamin B12 metabolism. While earlier studies could only infer cofactor affinity indirectly, often by observing how ligand addition shifted protein stability [15] or, as in our previous experiments, by monitoring changes in intrinsic fluorescence upon incremental ligand addition [21], here, by measuring the heat released during the titration of the ligand into the protein solution, we directly obtained the binding isotherms for AdoCbl binding to MMACHC, yielding K_d values, together with the complete thermodynamic binding profile (Gibbs energy, enthalpy, and entropy of binding).

These measurements allowed us to correlate binding affinity with the stabilizing effect of the vitamin, which we assessed using a dye-free spectroscopic technique such as CD (Fig. 1b). In addition, the direct ITC measurement of binding thermodynamics provides a more robust determination of how the R161Q mutation, although located far from B12 binding site, considerably impair the AdoCbl binding to the protein. The impaired binding to AdoCbl could result from alterations in the overall protein fold and the global stability induced by the mutation, as previously investigated by using an extrinsic dye fluorescence-based thermal shift assay or turbidity assays [15,43]. In those works, by using a single transition model for analyzing the thermal unfolding process, the MMACHC-R161Q mutant was shown to unfold at a temperature about 2 °C lower than the wild-type protein. In the present work, we investigated the MMACHC-WT and MMACHC-R161Q global stability by using DSC. Notably, our DSC data allowed us to unveil a more complex unfolding process in both proteins with the presence of two conformational intermediate states (Fig. 2, Table 2).

While the three-state model for wild-type protein denaturation was originally proposed by Froese et al. as a theoretical framework based on the shape of the denaturation curve [15], our study provides experimental verification of this model. Moreover, DSC revealed that the MMACHC-R161Q mutant unfolds according to a two-transition model as well. However, while the two transitions in the wild-type protein occur at very distinct temperatures, giving rise to separate peaks in the DSC thermogram, the two unfolding temperatures in the mutant are very close, resulting in a broader single apparent peak. This result suggests that the intermediate conformational states could show a different stability or be differently populated, leading to an unfolding process with different cooperativity. Comparable unfolding enthalpy and temperature values for the first transition suggest that the first intermediate is stabilized to a similar extent relative to the folded state in both proteins (Fig. 3a). In contrast, the reduced unfolding enthalpy and temperature observed for the second transition in the mutant suggest that its principal intermediate state is either less stable or structurally distinct from that of the wild type, potentially contributing to a more destabilized folding process overall as can be also observed when calculating the populations of the different states as a function of temperature for MMACHC-WT and MMACHC-R161Q (Fig. 3b).

From that detailed description, it can be seen that, although the MMACHC-R161Q populates significantly both intermediate states, the folding cooperativity of MMACHC-WT is much lower than that of MMACHC-R161Q, because of the larger separation between the folded and unfolded states in temperature for the former, a gap that is occupied by a considerably populated first intermediate.

We also demonstrated that, unlike the wild type, these closer transitions in the mutant were not detectable by a spectroscopic assay such as CD (Fig. 1b), which could only resolve a single unfolding curve, thus confirming the power of using DSC in providing deeper insights into the protein conformational landscape. Differences in the intermediate conformational populations between the two proteins may underline the distinct isothermal denaturation curves observed by SYPRO Orange fluorescence emission upon incubation with the two apoproteins over time (Fig. 9). The specific affinities of the unfolding intermediates for the dye are responsible for the observed denaturation profile [42]. Differences in stability between the wild type and mutant proteins can also be detected by simulating temperature jumps using Molecular Dynamics. Although these jumps do not induce complete unfolding of the proteins, they provide insights into differences in intermediate unfolding conformations. Despite the loss in secondary structure between the two proteins, wild type and R161Q mutant, is similar, the RMSD of the mutant increased significantly over a simulation period of one microsecond compared to the wild type. This indicates greater instability in the mutant tertiary structure of unfolding conformational intermediates (Fig. 4a). This instability in the tertiary structure may be attributed to either a reduction in molecular compactness or an enhanced propensity for aggregation, as corroborated by DLS and SAXS experiments (Fig. 5).

Another key finding from our experiments was the reduced ability of MMACHC-R161Q to form dimers and tetramers compared to MMACHC-WT. It has been reported that MMACHC is able to form domain-swap dimers in the presence of AdoCbl, and, from these, also tetrameric structures can form [13,44]. Through native gel electrophoresis, size-exclusion chromatography, and light scattering, we found that, while MMACHC-R161Q retains the ability to form dimers, their abundance is reduced compared to the wild-type protein (Fig. 8, Table 3). This finding suggests that the changes in the Cbl-binding region as a consequence of its altered fold and stability render the MMACHC-R161Q unable to adopt the correct conformation to engage in subunit exchange, leading to a reduced dimerization efficiency. Additionally, native gel electrophoresis (Fig. 8a, b) revealed that, in the case of MMACHC-WT, the addition of GSH to the protein-Cbl complex further increased dimer and tetramer formation, highlighting the functional and structural interplay between different regions of the protein. Structural and biophysical studies have shown that protein dimerization plays a key role in regulating protein function [45]. Evidence from our experiments indicate that MMACHC dimers form in the presence of essential cofactors, such as vitamin B12 and GSH. These observations provide indirect support for the idea that dimer formation represents a structural protein reorganization, and an additional regulation mechanism, necessary for this enzyme's proper functioning. We believe that the inability to form dimers in a pathological mutant further supports this hypothesis, although it is clear that further experiments are needed to fully understand the exact

functional role of dimeric conformations.

Finally, our study sheds light on the potential role of betaine (*N*-trimethylglycine) in the context of cblC disease, offering a new perspective beyond its conventional metabolic effect. Clinically, betaine is an established adjunct therapy for cblC patients, primarily used to lower elevated homocysteine levels by serving as a methyl donor in the betaine-homocysteine methyltransferase pathway [5,10]. It is known that small organic osmolytes like betaine can stabilize proteins against thermal denaturation without specific binding. Betaine and related osmolytes are preferentially excluded from the protein surface, thus increasing the water activity and favoring the compact native conformation and preventing unfolding [46,47]. Given the reduced thermal stability exhibited by some mutant proteins involved in common inborn metabolic diseases, the use of chemical chaperones such as glycerol, proline, betaine, and trimethylamine N-oxide (TMAO) has been shown to partially rescue these proteins both in vitro and in vivo [40]. Our findings demonstrate that among the different tested osmolytes, only betaine increases the thermal stability of the MMACHC-R161Q mutant (Fig. 10) Moreover, our results show that betaine's general protein-stabilizing properties can partially restore the enzymatic activity, as assessed in vitro (Fig. 12). This represents a proof-of-principle that enhancing protein stability could be a viable strategy for improving the impaired enzymatic activity in cblC, as resulting from MMACHC pathological mutants. A potential next step from a therapeutic perspective could involve the identification of pharmacological chaperones — molecules capable to specifically bind to MMACHC mutants, increasing its thermal stability and stabilizing its correct folded and active state — through high-throughput screening of small-molecule libraries.

5. Conclusions

Summarizing, our study provides novel insights into the thermodynamics underlying MMACHC stability and the impact of disease-associated mutations on its folding, its oligomeric organization and cofactors-binding properties. The R161Q mutation impairs key protein functions, including GSH and AdoCbl binding, dimerization, and protein stability, which directly contribute to the reduced enzymatic activity. By elucidating these molecular changes, we also demonstrate the potential therapeutic benefit of using osmolytes, specifically betaine, to enhance the thermal stability of the mutant protein and partially restore its function. Our findings suggest that targeting protein stability, through the use of chemical chaperones or pharmacological agents, holds promise as a novel therapeutic strategy for cblC disease and other related inborn metabolic disorders. Further research, particularly into the identification of pharmacological chaperones, could pave the way for developing effective treatments aimed at stabilizing MMACHC and improving its function in cblC patients.

CRediT authorship contribution statement

Lisa Longo: Writing – review & editing, Writing – original draft, Visualization, Validation, Methodology, Investigation, Data curation. **Loredana Randazzo:** Writing – review & editing, Writing – original draft, Validation, Methodology, Investigation. **Michela Bollati:** Writing – review & editing, Methodology, Investigation. **Rita Carrotta:** Writing – review & editing, Methodology, Investigation, Formal analysis. **Maria Assunta Costa:** Writing – review & editing, Writing – original draft, Methodology, Investigation, Data curation. **Matteo De Rosa:** Writing – review & editing, Methodology, Investigation, Conceptualization. **Maria Rosalia Mangione:** Writing – review & editing, Visualization, Validation, Methodology, Investigation. **Vincenzo Martorana:** Writing – review & editing, Validation, Supervision, Methodology, Investigation, Formal analysis. **Giulia Culletta:** Writing – review & editing, Investigation. **Marco Tutone:** Writing – review & editing, Supervision, Investigation. **Eleonora Mari:** Writing – review & editing, Investigation. **Maria Grazia Ortore:** Writing – review & editing, Methodology, Investigation, Formal analysis. **Paula M. Garcia-Franco:** Writing – review & editing, Investigation. **Adrian Velazquez-Campoy:** Writing – review & editing, Writing – original draft, Supervision, Methodology, Formal analysis, Data curation. **Rosa Passantino:** Writing – review & editing, Writing – original draft, Validation, Supervision, Methodology, Investigation, Conceptualization. **Silvia Vilasi:** Writing – review & editing, Writing – original draft, Validation, Supervision, Methodology, Investigation, Conceptualization.

Funding

This research was supported by HCU Network America, the Organic Acidemia Association, and the cblC aps Associazione Italiana Acidemia Metilmalonica con Omocistinuria through the grant *"Identification of Compounds to Rescue MMACHC Functional Deficiency in cblC Disease"* (agreement dated April 14, 2022, protocol number CNR IBF 5/6/2022).

Further funding was provided by the Italian Ministry of University and Research (MUR), National Recovery and Resilience Plan (NRRP), MNESYS project (*PE0000006*), *A Multiscale Integrated Approach to the Study of the Nervous System in Health and Disease*, via the cascade funding mechanism of Spoke 6, under the *RONEND* project (PRR.AP015.085 MNESYS_BaC_Spoke6_RONEND).

Declaration of competing interest

None.

Acknowledgements

We thank CERIC-ERIC research infrastructure for providing us beamtime in Elettra Synchrotron (proposal number 20227167), and Heinz Amenitsch and Barbara Sartori for the experimental set-up and assistance.

This work was supported by MOSBRI, a project receiving funding from the European Union's Horizon 2020 Research and Innovation Program under grant agreement No. 101004806 (MOSBRI-2023-184). Technical support from Marta Asencio del Río and Sonia Vega from the MOSBRI BIFI-LACRIMA node is much appreciated.

We are grateful to Fabrizio Giambertone, Alessia Provenzano, and Antonio Sauro for their fundamental technical support.

We acknowledge a contribution from the Italian National Recovery and Resilience Plan (PNRR), M4C2, funded by the European Union – NextGenerationEU (Project IR0000011, CUP B51E22000150006, "EBRAINS-Italy") within a TNA activity.

Appendix A. Supplementary data

Supplementary data to this article can be found online at https://doi.org/10.1016/j.ymgme.2025.109150.

Data availability

Data will be made available on request.

References

[1] J.P. Lerner-Ellis, J.C. Tirone, P.D. Pawelek, C. Dore, J.L. Atkinson, D. Watkins, C. F. Morel, T.M. Fujiwara, E. Moras, A.R. Hosack, G.V. Dunbar, H. Antonicka, V. Forgetta, C.M. Dobson, D. Leclerc, R.A. Gravel, E.A. Shoubridge, J.W. Coulton, P. Lepage, J.M. Rommens, K. Morgan, D.S. Rosenblatt, Identification of the gene responsible for methylmalonic aciduria and homocystinuria, cblC type, Nat. Genet. 38 (2006) 93–100.

[2] J.P. Lerner-Ellis, N. Anastasio, J. Liu, D. Coelho, T. Suormala, M. Stucki, A. D. Loewy, S. Gurd, E. Grundberg, C.F. Morel, D. Watkins, M.R. Baumgartner, T. Pastinen, D.S. Rosenblatt, B. Fowler, Spectrum of mutations in MMACHC, allelic expression, and evidence for genotype-phenotype correlations, Hum. Mutat. 30 (2009) 1072–1081.

[3] C. Nogueira, C. Aiello, R. Cerone, E. Martins, U. Caruso, I. Moroni, C. Rizzo, L. Diogo, E. Leao, F. Kok, F. Deodato, M.C. Schiaffino, S. Boenzi, O. Danhaive,

C. Barbot, S. Sequeira, M. Locatelli, F.M. Santorelli, G. Uziel, L. Vilarinho, C. Dionisi-Vici, Spectrum of MMACHC mutations in Italian and Portuguese patients with combined methylmalonic aciduria and homocystinuria, cblC type Molecular genetics and metabolism, Mol. Genet. Metab. 93 (2008) 475–480.
[4] N. Carrillo-Carrasco, R.J. Chandler, C.P. Venditti, Combined methylmalonic acidemia and homocystinuria, cblC type. I. Clinical presentations, diagnosis and management, J. Inherit. Metab. Dis. 35 (2012) 91–102.
[5] M. Huemer, D. Diodato, B. Schwahn, M. Schiff, A. Bandeira, J.F. Benoist, A. Burlina, R. Cerone, M.L. Couce, A. Garcia-Cazorla, G. la Marca, E. Pasquini, L. Vilarinho, J.D. Weisfeld-Adams, V. Kozich, H. Blom, M.R. Baumgartner, C. Dionisi-Vici, Guidelines for diagnosis and management of the cobalamin-related remethylation disorders cblC, cblD, cblE, cblF, cblG, cblJ and MTHFR deficiency, J. Inherit. Metab. Dis. 40 (2017) 21–48.
[6] L. Bonafede, C.H. Ficicioglu, L. Serrano, G. Han, J.I.W. Morgan, M.D. Mills, B. J. Forbes, S.L. Davidson, G. Binenbaum, P.B. Kaplan, C.W. Nichols, P. Verloo, B. P. Leroy, A.M. Maguire, T.S. Aleman, Cobalamin C deficiency shows a rapidly progressing maculopathy with severe photoreceptor and ganglion cell loss, Invest. Ophthalmol. Vis. Sci. 56 (2015) 7875–7887.
[7] E. Kiessling, S. Notzli, V. Todorova, M. Forny, M.R. Baumgartner, M. Samardzija, J. Krijt, V. Kozich, C. Grimm, D.S. Froese, Absence of MMACHC in peripheral retinal cells does not lead to an ocular phenotype in mice, Bba-Mol. Basis Dis. 1867 (2021).
[8] D. Ricci, D. Martinelli, G. Ferrantini, S. Lucibello, M. Gambardella, G. Olivieri, D. Chieffo, D. Battaglia, D. Diodato, G. Iarossi, A.M. Donati, C. Dionisi-Vici, R. Battini, E.M. Mercuri, Early neurodevelopmental characterization in children with cobalamin C/defect, J. Inherit. Metab. Dis. 43 (2020) 367–374.
[9] J.D. Weisfeld-Adams, H.A. Bender, A. Miley-Akerstedt, T. Frempong, N.L. Schrager, K. Patel, T.P. Naidich, V. Stein, J. Spat, S. Towns, M.P. Wasserstein, I. Peter, Y. Frank, G.A. Diaz, Neurologic and neurodevelopmental phenotypes in young children with early-treated combined methylmalonic acidemia and homocystinuria, cobalamin C type, Mol. Genet. Metab. 110 (2013) 241–247.
[10] S. Fischer, M. Huemer, M. Baumgartner, F. Deodato, D. Ballhausen, A. Boneh, A. B. Burlina, R. Cerone, P. Garcia, G. Gokcay, S. Grunewald, J. Haberle, J. Jaeken, D. Ketteridge, M. Lindner, H. Mandel, D. Martinelli, E.G. Martins, K.O. Schwab, S. C. Gruenert, B.C. Schwahn, L. Sztriha, M. Tomaske, F. Trefz, L. Vilarinho, D. S. Rosenblatt, B. Fowler, C. Dionisi-Vici, Clinical presentation and outcome in a series of 88 patients with the cblC defect, J. Inherit. Metab. Dis. 37 (2014) 831–840.
[11] M.P. Mcrae, Betaine supplementation decreases plasma homocysteine in healthy adult participants: a meta-analysis, J. Chiropr. Med. 12 (2013) 20–25.
[12] M. Koutmos, C. Gherasim, J.L. Smith, R. Banerjee, Structural basis of multifunctionality in a vitamin B12-processing enzyme, J. Biol. Chem. 286 (2011) 29780–29787.
[13] D.S. Froese, T. Krojer, X. Wu, R. Shrestha, W. Kiyani, F. von Delft, R.A. Gravel, U. Oppermann, W.W. Yue, Structure of MMACHC reveals an arginine-rich pocket and a domain-swapped dimer for its B12 processing function, Biochemistry 51 (2012) 5083–5090.
[14] J. Kim, L. Hannibal, C. Gherasim, D.W. Jacobsen, R. Banerjee, A human vitamin B12 trafficking protein uses glutathione transferase activity for processing alkylcobalamins, J. Biol. Chem. 284 (2009) 33418–33424.
[15] D.S. Froese, S. Healy, M. McDonald, G. Kochan, U. Oppermann, F.H. Niesen, R. A. Gravel, Thermolability of mutant MMACHC protein in the vitamin B12-responsive cblC disorder, Mol. Genet. Metab. 100 (2010) 29–36.
[16] L. Liguori, M. Monticelli, M. Allocca, B.H. Mele, J. Lukas, M.V. Cubellis, G. Andreotti, Pharmacological chaperones: a therapeutic approach for diseases caused by destabilizing missense mutations, Int. J. Mol. Sci. 21 (2020).
[17] T. Damy, P. Garcia-Pavia, M. Hanna, D.P. Judge, G. Merlini, B. Gundapaneni, T. A. Patterson, S. Riley, J.H. Schwartz, M.B. Sultan, R. Witteles, Efficacy and safety of tafamidis doses in the Tafamidis in transthyretin cardiomyopathy clinical trial (ATTR-ACT) and long-term extension study, Eur. J. Heart Fail. 23 (2021) 277–285.
[18] M. Fiore, C. Picco, O. Moran, Correctors modify the bicarbonate permeability of F508del-CFTR, Sci. Rep. 10 (2020).
[19] T. Majtan, A.L. Pey, J. Ereno-Orbea, L.A. Martinez-Cruz, J.P. Kraus, Targeting cystathionine Beta-synthase Misfolding in Homocystinuria by small ligands: state of the art and future directions, Curr. Drug Targets 17 (2016) 1455–1470.
[20] A.L. Pey, M. Ying, N. Cremades, A. Velazquez-Campoy, T. Scherer, B. Thöny, J. Sancho, A. Martinez, Identification of pharmacological chaperones as potential therapeutic agents to treat phenylketonuria, J. Clin. Invest. 118 (2008) 2858–2867.
[21] R. Passantino, M.R. Mangione, M.G. Ortore, M.A. Costa, A. Provenzano, H. Amenitsch, R. Sabbatella, C. Alfano, V. Martorana, S. Vilasi, Investigation on a MMACHC mutant from cblC disease: The c.394C > T variant, Proteins Proteom. 1870 (2022).
[22] A. Juzeniene, Z. Nizauskaite, Photodegradation of cobalamins in aqueous solutions and in human blood, J. Photochem. Photobiol. B 122 (2013) 7–14.
[23] J. Sancho, The stability of 2-state, 3-state and more-state proteins from simple spectroscopic techniques. plus the structure of the equilibrium intermediates at the same time, Arch. Biochem. Biophys. 531 (2013) 4–13.
[24] I. Jelesarov, H.R. Bosshard, Isothermal titration calorimetry and differential scanning calorimetry as complementary tools to investigate the energetics of biomolecular recognition, J. Mol. Recognit. 12 (1999) 3–18.
[25] M.J. Abraham, T. Murtola, R. Schulz, S. Páll, J.C. Smith, B. Hess, E. Lindahl, GROMACS: High performance molecular simulations through multi-level parallelism from laptops to supercomputers, SoftwareX 1 (2015) 19–25.
[26] J. Huang, A.D. MacKerell, CHARMM36 all-atom additive protein force field: validation based on comparison to NMR data, J. Comput. Chem. 34 (2013) 2135–2145.
[27] W. Humphrey, A. Dalke, K. Schulten, VMD: Visual molecular dynamics, J. Mol. Graph. Model. 14 (1996) 33–38.
[28] E.F. Pettersen, T.D. Goddard, C.R.C. Huang, E.E.C. Meng, G.S. Couch, T.I. Croll, J. H. Morris, T.E. Ferrin, UCSF ChimeraX: Structure visualization for researchers, educators, and developers, Protein Sci. 30 (2021) 70–82.
[29] R. Gowers, M. Linke, J. Barnoud, T. Reddy, M. Melo, S. Seyler, J. Domański, D. Dotson, S. Buchoux, I. Kenney, O. Beckstein, MDAnalysis: A Python Package for the Rapid Analysis of Molecular Dynamics Simulations, 2016, pp. 98–105.
[30] P. Stepanek, The method and some applications, in: W. Brown (Ed.), Dynamic Light Scattering, Clarendon Press, Oxford, U.K., 1993.
[31] P.N. Pusey, Introduction to scattering experiments, in: T.Z.P. Lindner (Ed.), Neutrons, X-Rays, and Light: Scattering Methods Applied to Soft Condensed Matter, Elsevier, Amsterdam, 2002, pp. 3–22.
[32] R. Haider, B. Sartori, A. Radeticchio, M. Wolf, S. Dal Zilio, B. Marmiroli, H., Amenitsch, microDrop: a system for high-throughput small-angle X-ray scattering measurements of microlitre samples, J. Appl. Crystallogr. 54 (2021) 132–141.
[33] Y.T. Chen, H.Y. Lu, N. Zhang, Z.F. Zhu, S.Q. Wang, M.H. Li, PremPS: predicting the impact of missense mutations on protein stability, PLoS Comput. Biol. 16 (2020).
[34] S. Vilasi, L. Longo, L. Randazzo, M. Bollati, R. Carrotta, M.A. Costa, M. De Rosa, M. R. Mangione, V. Martorana, M. Milani, M.G. Ortore, M. Tutone, R. Passantino, Studying an orphan disease by a biophysical approach: The case of cblC, Nuovo Cim. C-Colloq C 47 (2024).
[35] Y.T. Meharenna, T.L. Poulos, Using molecular dynamics to probe the structural basis for enhanced stability in thermal stable cytochromes P450, Biochemistry 49 (2010) 6680–6686.
[36] M. Plesa, J. Kim, S.G. Paquette, H. Gagnon, C. Ng-Thow-Hing, B.F. Gibbs, M. A. Hancock, D.S. Rosenblatt, J.W. Coulton, Interaction between MMACHC and MMADHC, two human proteins participating in intracellular vitamin B(1)(2) metabolism, Mol. Genet. Metab. 102 (2011) 139–148.
[37] M. Bastos, O. Abian, C.M. Johnson, F. Ferreira-da-Silva, S. Vega, A. Jimenez-Alesanco, D. Ortega-Alarcon, A. Velazquez-Campoy, Isothermal titration calorimetry, Nat. Rev. Method Prime 3 (2023).
[38] M. Ruetz, A. Shanmuganathan, C. Gherasim, A. Karasik, R. Salchner, C. Kieninger, K. Wurst, R. Banerjee, M. Koutmos, B. Kräutler, Antivitamin B12 inhibition of the human B12 -processing enzyme CblC: crystal structure of an inactive ternary complex with glutathione as the cosubstrate, Angew. Chem. Int. Edit. 56 (2017) 7387–7392.
[39] C. JTR, A Clinical Guide to Inherited Metabolic Diseases, 2005.
[40] W.W. Yue, From structural biology to designing therapy for inborn errors of metabolism, J. Inherit. Metab. Dis. 39 (2016) 489–498.
[41] F.H. Niesen, H. Berglund, M. Vedadi, The use of differential scanning fluorimetry to detect ligand interactions that promote protein stability, Nat. Protoc. 2 (2007) 2212–2221.
[42] R.W. Sarver, J.M. Rogers, D.E. Epps, Determination of ligand-MurB interactions by isothermal denaturation: application as a secondary assay to complement high throughput screening, J. Biomol. Screen. 7 (2002) 21–28.
[43] C. Gherasim, M. Ruetz, Z. Li, S. Hudolin, R. Banerjee, Pathogenic mutations differentially affect the catalytic activities of the human B12-processing chaperone CblC and increase futile redox cycling, J. Biol. Chem. 290 (2015) 11393–11402.
[44] D.S. Froese, J. Kopec, F. Fitzpatrick, M. Schuller, T.J. McCorvie, R. Chalk, T. Plessl, V. Fettelschoss, B. Fowler, M.R. Baumgartner, W.W. Yue, Structural insights into the MMACHC-MMADHC protein complex involved in vitamin B12 trafficking, J. Biol. Chem. 290 (2015) 29167–29177.
[45] N.J. Marianayagam, M. Sunde, J.M. Matthews, The power of two: protein dimerization in biology, Trends Biochem. Sci. 29 (2004) 618–625.
[46] T.O. Street, D.W. Bolen, G.D. Rose, A molecular mechanism for osmolyte-induced protein stability (vol 103, pg 13997, 2006), Proc. Natl. Acad. Sci. USA 103 (2006) 17064.
[47] R. Dandage, A. Bandyopadhyay, G.G. Jayaraj, K. Saxena, V. Dalal, A. Das, K. Chakraborty, Classification of chemical chaperones based on their effect on protein folding landscapes, ACS Chem. Biol. 10 (2015) 813–820.